RESEARCH ARTICLE

Single-Cell Tracking Reveals Antibiotic-Induced Changes in Mycobacterial Energy Metabolism

Željka Maglica,* Emre Özdemir,* John D. McKinney

School of Life Sciences, Swiss Federal Institute of Technology in Lausanne (EPFL), Lausanne, Switzerland

* Present address: Željka Maglica, Department of Molecular Medicine and Biotechnology, School of Medicine, University of Rijeka, Rijeka, Croatia; Emre Özdemir, Technical University of Denmark, Hørsholm, Denmark.

ABSTRACT **ATP is a key molecule of cell physiology, but despite its importance, there are currently no methods for monitoring single-cell ATP fluctuations in live bacteria. This is a major obstacle in studies of bacterial energy metabolism, because there is a growing awareness that bacteria respond to stressors such as antibiotics in a highly individualistic manner. Here, we present a method for long-term single-cell tracking of ATP levels in *Mycobacterium smegmatis* based on a combination of microfluidics, time-lapse microscopy, and Förster resonance energy transfer (FRET)-based ATP biosensors. Upon treating cells with antibiotics, we observed that individual cells undergo an abrupt and irreversible switch from high to low intracellular ATP levels. The kinetics and extent of ATP switching clearly discriminate between an inhibitor of ATP synthesis and other classes of antibiotics. Cells that resume growth after 24 h of antibiotic treatment maintain high ATP levels throughout the exposure period. In contrast, antibiotic-treated cells that switch from ATP-high to ATP-low states never resume growth after antibiotic washout. Surprisingly, only a subset of these nongrowing ATP-low cells stains with propidium iodide (PI), a widely used live/dead cell marker. These experiments also reveal a cryptic subset of cells that do not resume growth after antibiotic washout despite remaining ATP high and PI negative. We conclude that ATP tracking is a more dynamic, sensitive, reliable, and discriminating marker of cell viability than staining with PI. This method could be used in studies to evaluate antimicrobial effectiveness and mechanism of action, as well as for high-throughput screening.**

IMPORTANCE **New antimicrobials are urgently needed to stem the rising tide of antibiotic-resistant bacteria. All antibiotics are expected to affect bacterial energy metabolism, directly or indirectly, yet tools to assess the impact of antibiotics on the ATP content of individual bacterial cells are lacking. The method described here for single-cell tracking of intracellular ATP in live bacteria has many advantages compared to conventional ensemble-averaged assays. It provides a continuous real-time readout of bacterial ATP content, cell vitality, and antimicrobial mechanism of action with high temporal resolution at the single-cell level. In combination with high-throughput microfluidic devices and automated microscopy, this method also has the potential to serve as a novel screening tool in antimicrobial drug discovery.**

Received 5 November 2014 **Accepted** 28 December 2014 **Published** 17 February 2015

Citation Maglica Ž, Özdemir E, McKinney JD. 2015. Single-cell tracking reveals antibiotic-induced changes in mycobacterial energy metabolism. mBio 6(1):e02236-14. doi: 10.1128/mBio.02236-14.

Editor Carol A. Nacy, Sequella, Inc.

Address correspondence to Željka Maglica, zeljka.maglica@gmail.com.

Methods for high-throughput screening (HTS) in antibacterial drug discovery can be broadly categorized as target based or cell based (1). Despite substantial investment in target-based HTS campaigns by the pharmaceutical industry during the past decade, this approach has been largely unsuccessful (2). In part, this failure can be attributed to the high frequency of inhibitors whose activity against their molecular targets *in vitro* does not translate to antibacterial activity *in vivo*. Live-cell screening also offers the potential to query all essential functions simultaneously, rather than one at a time. These considerations have refocused attention on cell-based HTS as a potentially more productive approach (3). For example, bedaquiline (formerly TMC207), a novel inhibitor of mycobacterial ATP synthase, was discovered by screening compound libraries against living cells of *Mycobacterium smegmatis*, a nonpathogenic relative of the human pathogen *Mycobacterium tuberculosis* (4). This cell-based approach not only led to the identification and validation of a new target for antibacterial drug discovery (ATP synthase) but also produced the first new antituberculosis drug to receive regulatory approval from the U.S. Food and Drug Administration since rifampin was approved in 1971 (5).

Ongoing efforts to identify new and more effective antimicrobials are hindered by the inherent limitations of conventional cell culture assays, which provide ensemble-averaged measurements of bacterial phenotypes. These assays obscure the underlying cell-to-cell variation of the phenotype being measured, which is a critical shortcoming, because all antibiotics exhibit fractional killing, whereby a subpopulation of phenotypic variants (called "persisters") escape killing although they are not genetically resistant to the antibiotic (6). Conventional assays are also inadequate to

identify, let alone study, subpopulations of nongrowing but metabolically active (NGMA) cells, which have been implicated in chronic infections (7, 8), and they do not permit the temporal tracking of phenotypic fluctuations in individual cells. For example, these methods cannot distinguish whether a 50% drop in ensemble-averaged ATP content following drug exposure is due to 100% depletion of ATP in 50% of cells or 50% depletion in 100% of cells, nor can they reveal whether these changes are reversible or irreversible at the single-cell level.

Fluorescent indicators have become an indispensable tool for visualizing phenotypes at the single-cell level, but there are surprisingly few such indicators available for studies of bacterial physiology and metabolism. Bacteria can be stained with fluorescent indicator dyes, such as propidium iodide (PI), but indicator dyes often affect cell physiology and are not suitable for long-term studies of live bacteria. In recent years, genetically encoded biosensors based on Förster resonance energy transfer (FRET) have been developed for real-time single-cell measurements of specific target metabolites in living eukaryotic cells (9, 10). To date, however, application of FRET-based biosensors to the study of microbial metabolism has been limited. FRET-based biosensors for oxygen, citrate, pentose, and ATP have been used in batch-culture studies of *Escherichia coli* (11–14), and short-term time-lapse microscopy has been used to monitor spatial and temporal changes of cyclic di-GMP in *Caulobacter crescentus* and *Pseudomonas aeruginosa* (15). Although ATP homeostasis is among the most important of all cellular activities, we are not aware of any assay system permitting long-term temporal tracking of ATP fluctuations in single bacterial cells. This information is vital for understanding the impact of an antibiotic on bacterial energy metabolism and how this translates into antibacterial activity. Antibiotics can affect intracellular ATP levels either by inhibiting ATP synthase directly (4) or by disrupting the membrane electrochemical potential, which is required for ATP synthase activity (16). Presumably, cell death would also result in rapid depletion of intracellular ATP levels, as the cytoplasmic pool of ATP in bacteria normally turns over with a half-life on the order of seconds (17).

Conventional methods for measuring intracellular ATP levels in bacteria require cell lysis and normalization of the signal to cell mass or cell numbers (18–21). Chemiluminescence-based bioassays can be used to measure ATP content of cell populations, but these methods are not suitable for single-cell studies or live-cell tracking, because cells must be permeabilized (22). In order to circumvent these limitations, we developed a method for single-cell tracking of ATP fluctuations in *Mycobacterium smegmatis*. This method is based on a combination of microfluidics, time-lapse microscopy, and genetically encoded FRET biosensors adapted from the ATeam series (23), which was recently developed for real-time ATP measurements in eukaryotic cells (24–26). The ATeam biosensors are based on the genetically encoded FRET pair of cyan and yellow fluorescent proteins (CFP and YFP, respectively) flanking the epsilon subunit of the *Bacillus subtilis* F_oF_1 ATP synthase, which binds ATP with high affinity and specificity.

Here, we demonstrate that this method can be used to track dynamic changes in ATP levels in bacteria exposed to antibiotics that target essential cellular processes, including ATP synthesis, cell wall biogenesis, DNA replication, RNA transcription, and protein translation. We found that the time required for ATP depletion in single cells depends on the mechanism of action of the corresponding antibiotic and varies markedly between individual cells. We also found that maintenance of high cytoplasmic ATP levels during antibiotic exposure is strongly correlated with survival of individual cells and their recovery following drug washout. These studies establish an integrated microfluidics-microscopy-biosensor system as a new tool to study bacterium-antibiotic interactions at single-cell resolution.

RESULTS

A bacterial biosensor for live-cell ATP measurements. We generated a reporter strain of *M. smegmatis* that constitutively expresses the biosensor ATeam1.03^{YEMK} (23). This FRET-based biosensor has medium affinity for ATP (K_d = 1.2 mM), which is within the range of cytoplasmic ATP level measured in bacterial cells cultured under growth-permissive conditions (27). Dynamic tracking of cytoplasmic ATP content is done by culturing the reporter bacteria (designated WT_MA, for "wild type, medium affinity") in a custom-made microfluidic device (28) and imaging the bacteria with the high-power objective (100×) on phase-contrast and fluorescence channels. Cells are grown in microfluidic flow medium containing acetate, a nonfermentable carbon source, in order to restrict ATP production to a single enzyme, ATP synthase (29). Time-lapse imaging of cells before and after exposure to a potent inhibitor of ATP synthase, bedaquiline (4), tracks the short- and long-term responses of individual WT_MA cells with high temporal resolution. FRET-based fluorescence of single cells is measured using a filter set optimized for excitation of CFP and emission of YFP ($CFP_{ex} \rightarrow YFP_{em}$). These FRET values are normalized to parallel measurements obtained with a filter set optimized for excitation and emission of YFP ($YFP_{ex} \rightarrow YFP_{em}$), in order to control for possible drift in expression of the ATP biosensor (30). Normalized values are expressed as the FRET/YFP ratio [($CFP_{ex} \rightarrow YFP_{em}$)/($YFP_{ex} \rightarrow YFP_{em}$)].

We found that single-cell ATeam1.03^{YEMK} expression (Fig. 1A, top row, and 1C, red traces) and FRET/YFP ratios are stable during growth and division in the absence of antibiotics (see Fig. S1B and Movie S1 in the supplemental material). Addition of bedaquiline causes a rapid (within 30 min) decrease of the FRET signal in all cells (Fig. 1A, middle row, and 1C, green traces) but has no effect on YFP fluorescence intensity. The resulting decrease of the FRET/YFP ratio demonstrates that changes in intracellular ATP can be monitored in real time at the single-cell level in WT_MA bacteria (Fig. 1A, bottom row, and 1D, blue traces). We define the cellular ATP status before and after the bedaquiline-induced decrease in FRET/YFP ratio as ATP high (range, 0.85 to 1.20) and ATP low (range, 0.50 to 0.75), respectively. These transitions can also be observed in images where FRET and YFP signals are merged rather than divided (Fig. 1B, middle). As the latter representation allows easier differentiation of individual cells than ratiometric images (Fig. 1B, right), movies derived from both representations are included in the supplemental material.

We compared the biosensor-based single-cell results with bulk measurements of intracellular ATP levels in WT_MA cells using the commercial BacTiter-Glo assay (Fig. S1A). Similar to the biosensor-based single-cell observations, we found that bulk ATP levels decline sharply within 30 min of bedaquiline exposure, and once ATP levels fall below the detection limit (0.1 nM), they remain unchanged thereafter. The BacTiter-Glo assay reports a 50% decrease in ATP levels during the first 10 min of bedaquiline exposure, whereas our biosensor-based measurements indicate that ATP levels are stable during this interval. This apparent discrep-

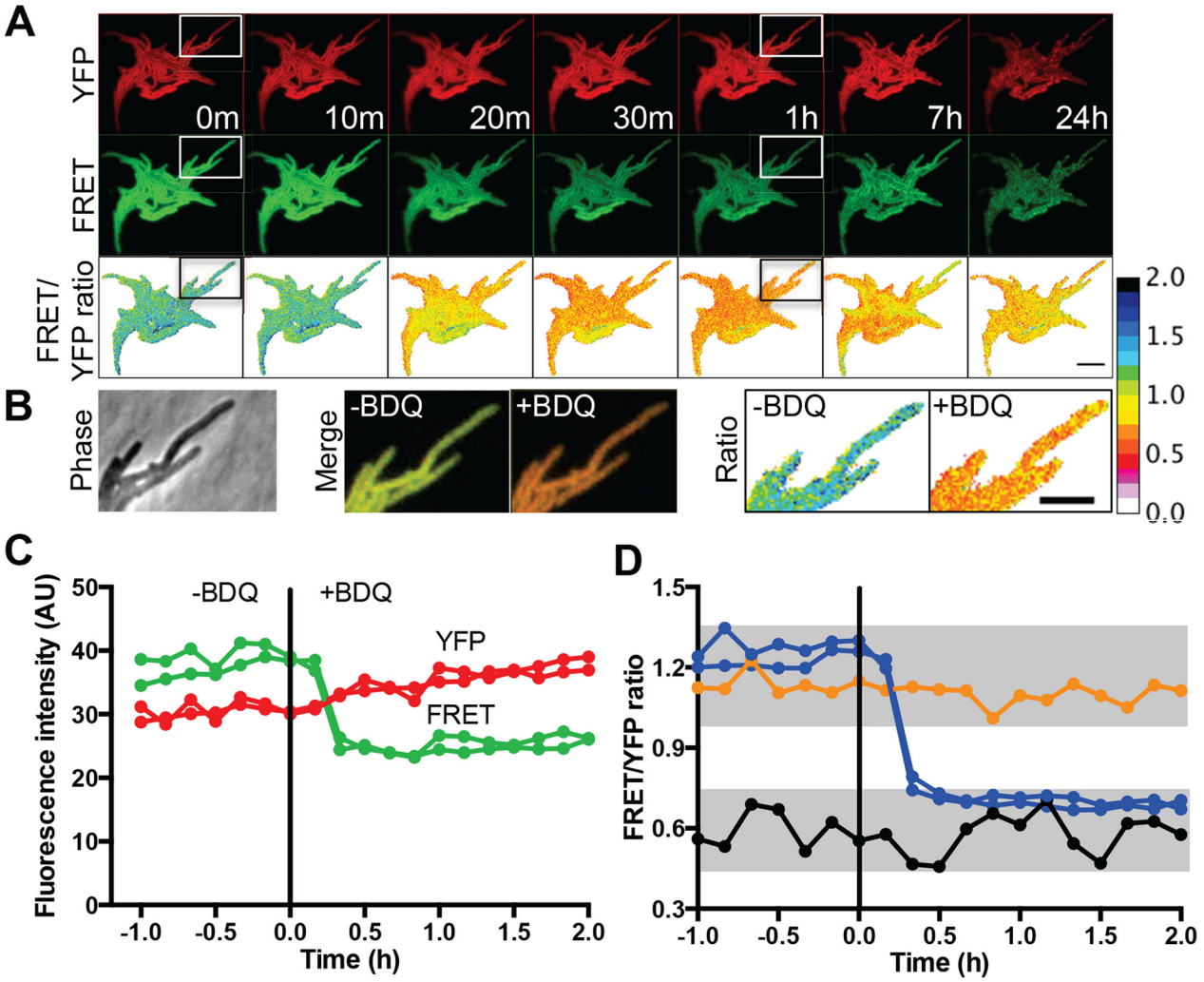

FIG 1 Real-time measurements of single-cell ATP using genetically encoded biosensors. Wild-type *M. smegmatis* expressing ATeam biosensors with high (WT_HA), medium (WT_MA), or low (WT_LA) affinity for ATP was used. Cells were grown in minimal-acetate medium in a microfluidic device with addition of bedaquiline (5 μg/ml) at time zero. Phase-contrast and fluorescence images were recorded at 10-min intervals. See Movie S1 in the supplemental material. (A) WT_MA cells. Representative image series recorded on the YFP (top) or FRET (middle) channel. Ratiometric FRET/YFP images (bottom) are pseudocolored. Numbers indicate time elapsed. Scale bar, 5 μm. (B) WT_MA cells. Representative images were recorded immediately before (–BDQ) or 1 h after (+BDQ) addition of bedaquiline to the flow medium. Images are zoomed from the boxed area in panel A. (Left) Phase-contrast image; (middle) merged images recorded on FRET (green) and YFP (red) channels; (right) pseudocolored ratiometric FRET/YFP images. Scale bar, 3 μm. (C) WT_MA cells. Time traces of fluorescence intensities of two representative cells, recorded on FRET (green lines) and YFP (red lines) channels, are shown. The vertical line represents time of bedaquiline addition. (D) Time traces of FRET/YFP ratios of WT_HA (orange), WT_MA (blue), and WT_LA (black) reporter strains. Ranges of the FRET/YFP ratios corresponding to high-ATP and low-ATP states are highlighted in grey.

ancy might reflect the unavoidable delay (5 to 10 min) in collecting and processing samples for the BacTiter-Glo bulk assay compared to the real-time measurements provided by the biosensor-based single-cell assay. Also, as the ATeam1.03^{YEMK} biosensor has a relatively high affinity for ATP, the kinetic lag after bedaquiline addition might reflect the time required for intracellular ATP to fall below saturating levels. In both assays, the decline in ATP levels occurs on the order of minutes rather than seconds. Given the extremely rapid turnover of the ATP pool in bacteria, the relatively slow decay in ATP levels in bedaquiline-treated cells might reflect the time required to deplete alternative energy sources, such as polyphosphate. Comparable kinetics of ATP depletion, on a time scale of minutes, occur in HeLa cells expressing the ATeam1.03 biosensor (K_d = 3.3 mM) after simultaneous addition of inhibitors of glycolysis and oxidative phosphorylation (23).

The FRET/YFP fluorescence ratio of the ATeam1.03^{YEMK} biosensor is dependent not only on the ATP concentration but also on the reporter's affinity for ATP. Under the same conditions, the ratio is expected to be higher for a reporter with high ATP affinity than a reporter with low ATP affinity. We tested this prediction by repeating experiments with control strains expressing ATP biosensors with high affinity (ATeam3.10; K_d = 7.4 μM) or low affinity (ATeam1.03^{KK}; K_d > 10 mM) (23), which we designated WT_HA and WT_LA, respectively. The FRET/YFP ratios of the WT_HA and WT_LA strains do not overlap and are easily distinguishable (Fig. 1D, orange and black traces, respectively). In contrast to the WT_MA reporter strain, fluorescence output of the

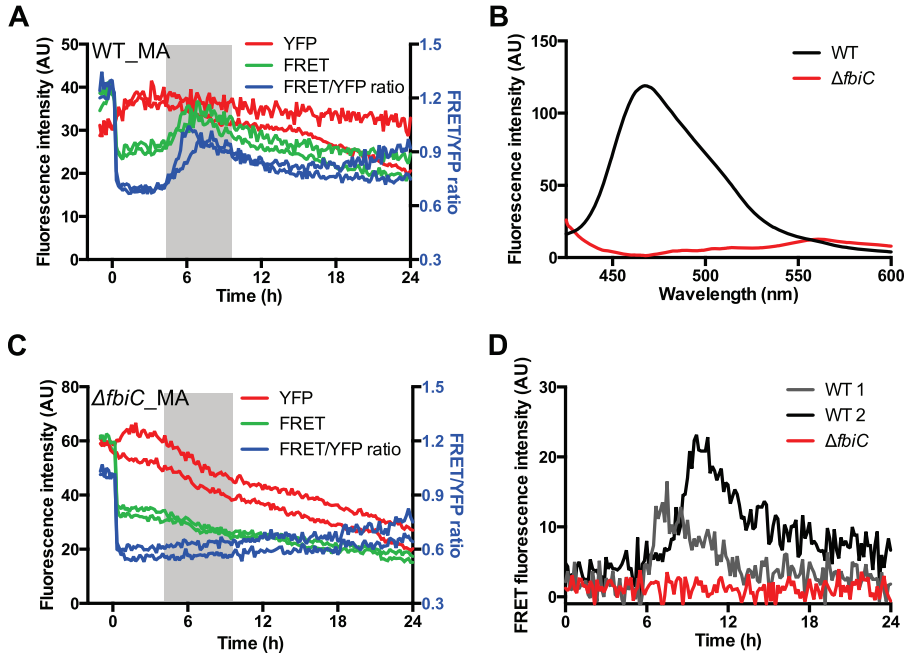

FIG 2 Antibiotic-induced cyan autofluorescence eliminated by deletion of *fbiC*. Strains used in each experiment are indicated in the top corner of each panel. Cells were cultured in minimal-acetate medium in a microfluidic device with addition of bedaquiline (5 μg/ml) at time zero. (A) Time traces of FRET (green) and YFP (red) fluorescence and FRET/YFP ratio (blue) of two representative cells from Movie S1 in the supplemental material. The time interval of transient FRET fluorescence increase is indicated in gray. (B) Emission spectra of wild-type (black) and Δ*fbiC* (red) strains recorded at an excitation wavelength of 405 nm. (C) Time traces of FRET (green) and YFP (red) fluorescence intensity and FRET/YFP ratio (blue) of two representative Δ*fbiC*_MA cells from Movie S3. (D) Time traces of autofluorescence intensity on the FRET channel of two representative wild-type cells (black and gray) and a typical Δ*fbiC* cell (red) from Movie S2.

WT_HA and WT_LA control strains is not affected by bedaquiline. These results confirm that there are no other cellular changes, besides the decrease in cytoplasmic ATP levels, affecting fluorescence output from the ATeam1.03^{YEMK} reporter in bedaquiline-stressed cells. In unstressed cells, the FRET/YFP ratios in the WT_MA and WT_HA strains are similar, suggesting that in both cases the biosensor is saturated with ATP. In bedaquiline-treated cells, the FRET/YFP ratio in the WT_MA strain declines to the same level as the WT_LA strain, suggesting that in both cases the biosensor is in the ATP-free form. The technical limitations of biosensors based on pairs of fluorescent proteins that mature and degrade at different rates may limit the accuracy of the ATeam1.03^{YEMK} biosensor in measuring absolute ATP concentrations in single cells (14). However, these issues are not limiting for the applications described in this study, which are based on measurements of relative ATP concentrations in single cells before and after antibiotic exposure in order to detect switching from the ATP-saturated form to the ATP-free form.

An F420-deficient reporter strain with reduced cyan autofluorescence. The FRET/YFP ratio remains constant for several hours after bedaquiline addition; however, after 5 to 10 h, we consistently observed a transient increase in the FRET channel and consequently in the FRET/YFP ratio (Fig. 2A; also, see Movie S1 in the supplemental material). This increase does not represent a true rise in ATP levels, because it also occurs in cells that express reporters with low and high affinity for ATP (see Fig. S1C) as well as cells that do not encode an ATP biosensor (Fig. 2D, black and grey traces; also, see Movie S2 [left]). This spurious increase in the FRET signal, due to background autofluorescence, is problematic because it could mask true time-dependent variation in ATP levels.

Cyan autofluorescence in mycobacteria is thought to be due to coenzyme F420 (31), whose biosynthesis is catalyzed by FbiC (32). We find that deletion of the *fbiC* gene markedly reduces cyan autofluorescence (Fig. 2B, red trace) and eliminates the bedaquiline-induced increase in autofluorescence on the FRET channel (Fig. 2D, red trace; also, see Movie S2 [right]), confirming that F420 is the primary source of cyan autofluorescence in *M. smegmatis*. Similar to wild-type cells, autofluorescence of Δ*fbiC* cells on the YFP channel is close to zero (see Fig. S1E). As most FRET biosensors are based on CFP/YFP FRET couples, the Δ*fbiC* strain will be broadly useful in applications involving CFP/YFP-based biosensors.

The wild-type and Δ*fbiC* strains are equally sensitive to antibiotics that inhibit essential cellular processes, including ATP synthesis, cell wall biogenesis, RNA transcription, protein translation, and DNA replication (see Fig. S1F in the supplemental material). Furthermore, the initial kinetics of FRET/YFP decline after bedaquiline exposure are indistinguishable in wild-type and Δ*fbiC* cells expressing the ATeam1.03^{YEMK} biosensor (see Fig. S1D). These results confirm that the Δ*fbiC* strain background is suitable for studies of antibiotic-mediated effects on bacterial physiology. The bedaquiline-induced cyan autofluorescence that we observe in wild-type cells does not occur in Δ*fbiC* ATeam1.03^{YEMK} cells (Δ*fbiC*_MA) (Fig. 2C, green traces; also, see Movie S3 in the supplemental material), demonstrating that the Δ*fbiC*_MA reporter strain can be used for long-term measurements of ATP content (FRET/YFP ratios) in antibiotic-treated cells (Fig. 2C, blue traces).

Differential kinetics of ATP depletion in antibiotic-treated bacteria. The rapid decline in ATP levels (FRET/YFP ratios) in bedaquiline-treated Δ*fbiC*_MA reporter cells presumably reflects the mechanism of action of this antimicrobial, which targets ATP

synthase. We also assessed the impact on ATP levels of antibiotics that inhibit other essential molecular targets, including isoniazid (fatty acid synthase II), streptomycin (ribosome 30S subunit), rifampin (RNA polymerase), and ciprofloxacin (DNA gyrase). In these experiments, Δ*fbiC*_MA cells are cultured in a microfluidic device, exposed to the antibiotic for 24 h, and then allowed to recover for another 24 h in the absence of antibiotic (see Movies S4 to S7 in the supplemental material). Although all antibiotics cause cell growth arrest, they do so with highly diverse kinetics. For example, bedaquiline causes immediate growth arrest, whereas ciprofloxacin-treated cells continue to grow for many hours in the presence of the antibiotic (see Fig. S2A in the supplemental material). Antibiotic exposure also influences YFP fluorescence. While most antibiotics cause a slow decline in YFP signal, for isoniazid there is an initial increase during the first ~5 h of exposure (see Fig. S2A).

All of the antibiotics that we tested cause a sharp downshift in FRET/YFP ratios in a small or large fraction of cells (depending on the antibiotic), indicating depletion of intracellular ATP, albeit with variable and delayed kinetics compared to bedaquiline (Fig. 3A). In each case, individual cells undergo a rapid switch from ATP-high to ATP-low states with FRET/YFP ratios similar to those in bedaquiline-treated cells (Fig. 3B). In most cells, the ATP switch (high to low) is a one-time-only event, but approximately 50% of the cells exposed to streptomycin and a smaller fraction of cells exposed to rifampin or ciprofloxacin (4% and 1%, respectively) underwent one or more rapid high-low-high fluctuations (see Fig. S2C in the supplemental material). We define ATP switching as the time when the transition from the ATP-high state to the ATP-low state stabilizes.

Although all tested antibiotics caused ATP depletion, the frequency and dynamics of ATP switching were highly variable (Fig. 3C). At opposite ends of the spectrum are bedaquiline, which induces switching in 100% of cells shortly after exposure (less than 30 min), and isoniazid, which induces switching in only a small fraction of cells, even after 48 h of exposure (Fig. 3C). The other antibiotics that we tested (rifampin, streptomycin, and ciprofloxacin) induce switching in approximately 90% of cells within 48 h, beginning 8 to 10 h after addition of the antibiotic to the flow medium (Fig. 3C). ATP switching continues during the postantibiotic recovery period for a large fraction of streptomycin-treated cells and a much smaller fraction of cells treated with rifampin or ciprofloxacin. The median switching time and the distribution of switching times in single cells are different for each of the five antibiotics that we tested, and there is little or no correlation in switching times between sibling cells derived from the same mother cell (see Fig. S2B in the supplemental material). Although isoniazid drives ATP switching in only a small number of cells, a modest decrease in the FRET/YFP ratio occurs in all isoniazid-treated cells (see Fig. S2D). These results demonstrate that antibiotics with different mechanisms of action can be differentiated based on the timing and magnitude of their effect on intracellular ATP levels.

ATP switching correlates with membrane permeability barrier breakdown. Propidium iodide (PI) is a membrane-impermeant DNA-intercalating agent that is commonly used as a selective stain to detect "dead" cells with damaged membrane permeability barriers. Due to its ability to accumulate gradually within live cells during prolonged incubation (33), which can have undesirable effects on cell physiology, PI staining is not well suited for continuous time-lapse studies, and it is typically used as an endpoint assay (4, 33, 34). In time-lapse experiments, we assessed the viability of antibiotic-treated cells by pulse-labeling cells with PI for 30 min after 24 h of antibiotic exposure and again for 30 min following an additional 24 h of postantibiotic recovery (Fig. 4A and B; also, see Fig. S2E in the supplemental material). We routinely observed that the fraction of PI-positive cells is higher at 48 h than at 24 h, indicating that many cells lose their membrane integrity during the postantibiotic recovery period. As with ATP switching, we observe substantial differences between different classes of antibiotics with respect to the timing and magnitude of PI staining. Again, bedaquiline and isoniazid represent opposite ends of the spectrum, generating 97% and 4% PI-positive cells, respectively, at the 48-h time point, while the other antibiotics that we tested generated intermediate numbers of PI-positive cells (Fig. 4B).

PI-positive cells are likely to be dead due to disrupted membrane integrity, and indeed we did not observe regrowth of any PI-positive cells after antibiotic washout. The status of PI-negative cells, on the other hand, is less clear. Among this subpopulation of cells, we looked for cells that recovered and resumed growth during the postantibiotic recovery period. After 24 h of exposure to bedaquiline or streptomycin, we did not observe recovery of any of these PI-negative cells, whereas a small fraction (less than 10%) of cells exposed to rifampin or ciprofloxacin resumed growth after drug washout (Fig. 4B). Nearly 50% of cells exposed to isoniazid resume growth after drug washout (Fig. 4B; also, see Movie S4 in the supplemental material), consistent with the relatively weak sterilizing activity of this compound against *M. smegmatis* (28).

In time-lapse microscopy experiments, we measured the FRET/YFP ratios of individual cells during 24 h of antibiotic exposure as a potential marker of cell fate. We found that the distribution of single-cell FRET/YFP ratios was bimodal, cleanly separating into cells with high values and cells with low values (Fig. 4C). Among cells that scored as PI positive and failed to resume growth after 24 h of drug exposure, the correlation between ATP switching (high to low) and PI positivity was >99% reliable ($n = 2{,}089$; 95% confidence level).

Biosensor-based ATP measurements provide additional information that PI staining does not. For example, the fraction of cells scored as PI negative at 24 h can be further subdivided into subpopulations with low or high ATP levels (Fig. 4D). Cells with low ATP levels never resumed growth after drug washout and were more likely to become PI positive during the 24-h postantibiotic recovery period (Fig. 4D, red symbols). Conversely, cells that resume growth after drug washout invariably maintained high ATP levels throughout the periods of antibiotic exposure and postantibiotic recovery (Fig. 4D, green symbols, and 4E). The correlation between maintenance of high ATP levels and viability (regrowth) is >99% reliable ($n = 659$; 95% confidence level). A substantial fraction of cells maintained high ATP levels yet failed to resume growth after antibiotic washout (Fig. 4D, grey symbols). Some of these cells became PI positive during the recovery period, which is 100% correlated with ATP switching (high to low) during the recovery period.

Carbon source dependency of ATP switching in bedaquiline-treated cells. In cells growing on carbohydrate substrates, cellular ATP is generated mainly by the operation of the tricarboxylic acid (TCA) cycle and oxidative phosphorylation (ATP synthase dependent), but some ATP also derives from glycolysis (ATP synthase

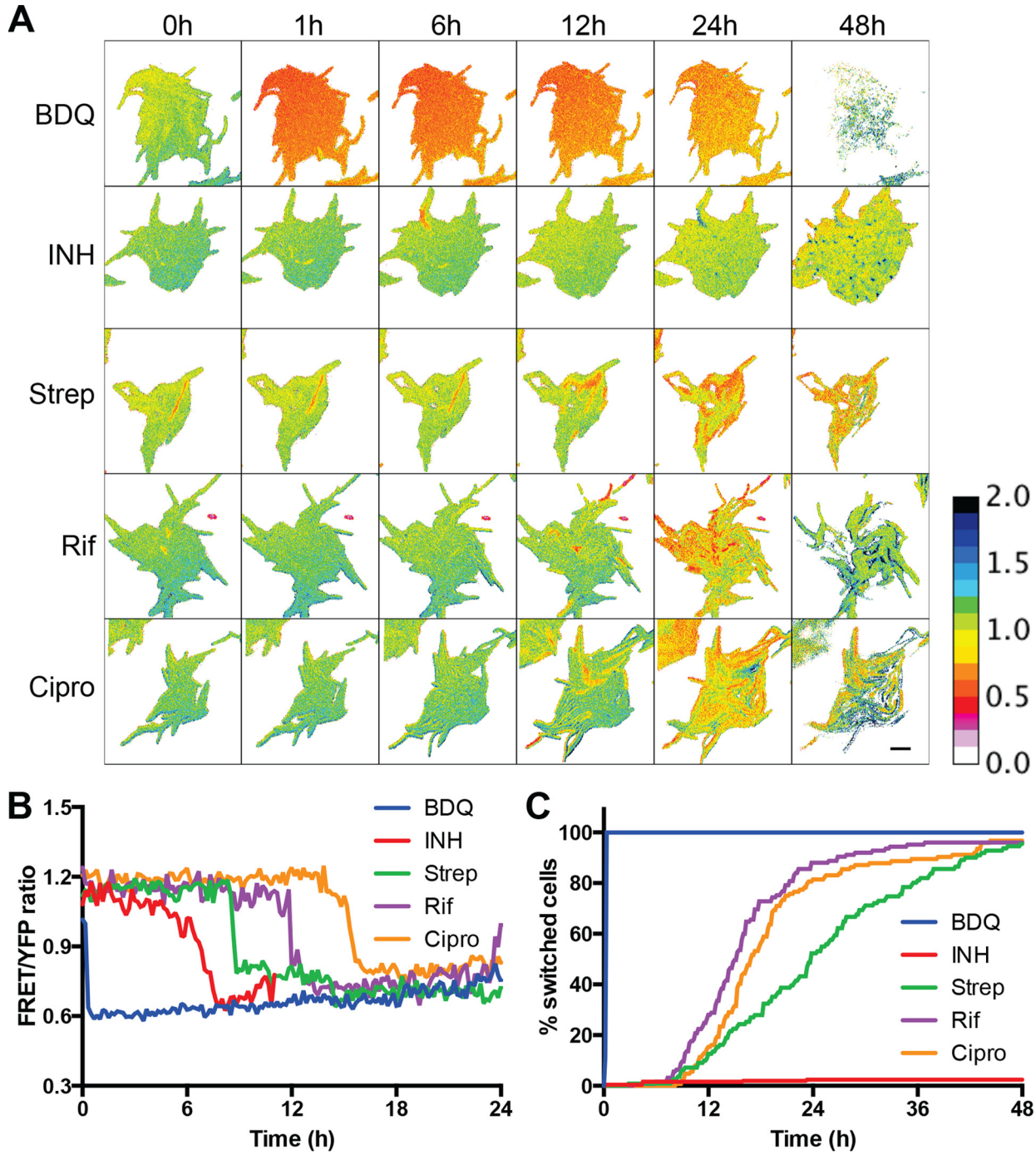

FIG 3 Discrimination of antibiotic classes based on kinetics of ATP switching in single cells. Δ*fbiC*_MA cells were cultured in minimal-acetate flow medium in a microfluidic device for 24 h before addition of antibiotic. Phase-contrast and fluorescence images were recorded at 10-min intervals for a 24-h exposure period with antibiotic followed by a 24-h recovery period without antibiotic. Antibiotic concentrations: bedaquiline (BDQ), 5 μg/ml; isoniazid (INH), 500 μg/ml; streptomycin (Strep), 125 μg/ml; rifampin (Rif), 200 μg/ml; ciprofloxacin (Cipro), 2.5 μg/ml. See Movies S3 to S7 in the supplemental material. (A) Representative FRET/YFP ratiometric images. Pixels are displayed as zero for denominator (YFP) values of <10 arbitrary units. Numbers indicate time elapsed. Scale bar, 5 μm. (B) Time traces of FRET/YFP ratios of selected cells during 24 h of drug exposure. Tracking of the isoniazid-exposed cell was performed only as long the YFP signal was above background. (C) Time traces of the percentage of cells undergoing ATP switching (high to low) after exposure to bedaquiline ($n = 277$), isoniazid ($n = 250$), streptomycin ($n = 111$), rifampin ($n = 125$), or ciprofloxacin ($n = 124$).

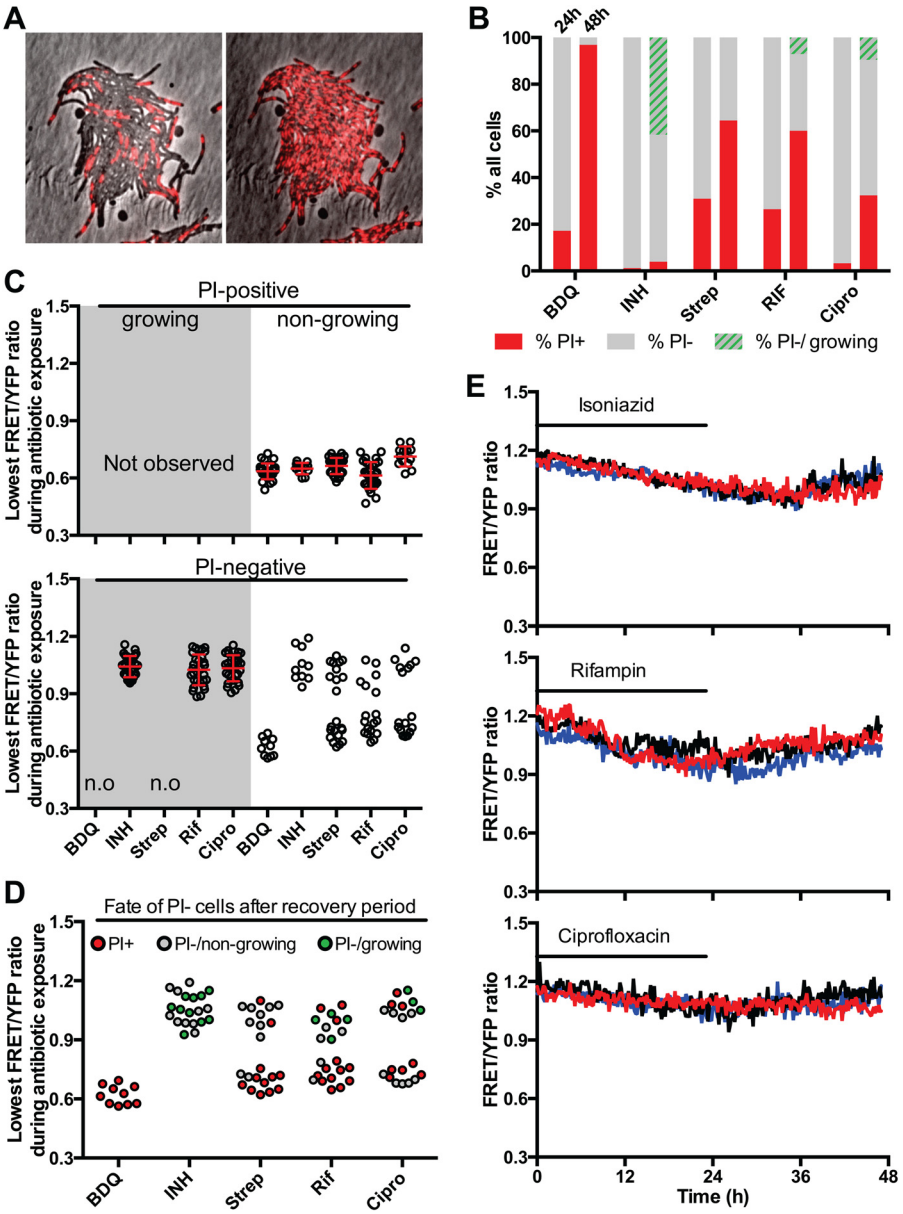

FIG 4 Antibiotic-induced ATP switching and PI staining as markers of live/dead status. Δ*fbiC*_MA cells were cultured in minimal-acetate flow medium, exposed to antibiotic, and analyzed as described in the legend to Fig. 3. See Movies S3 to S7 in the supplemental material. (A) Phase-contrast (grey) and fluorescence (red) images of bedaquiline-treated cells stained with PI at the end of the drug exposure period (24 h) and washout (48 h). (B) Fraction of PI-positive (red) and PI-negative (grey) cells at 24 and 48 h. Cells were scored as PI positive and nongrowing (red), PI negative and nongrowing (grey), or PI negative and growing (grey with green stripes). Data represent 20 movies from two independent experiments for each antibiotic: bedaquiline ($n = 483$), isoniazid ($n = 1,270$), streptomycin ($n = 1,178$), rifampin ($n = 1,021$), and ciprofloxacin ($n = 615$). (C) Lowest FRET/YFP ratios measured during antibiotic exposure (0 to 24 h). Cells were PI stained at 24 h and scored as PI positive (top) or PI negative (bottom) and growing or nongrowing during drug washout. Each symbol represents one cell ($n = 30$ per group except as noted). Red lines indicate means ± SD. (D) Lowest FRET/YFP ratios measured during antibiotic exposure (0 to 24 h) for cells that were scored as PI negative at 24 h. Cells were PI stained again at 48 h and scored as PI positive and nongrowing (red), PI negative and nongrowing (grey), or PI negative and growing (green). Each symbol represents one cell. (E) Time traces of FRET/YFP ratios of representative cells (three per antibiotic) that resumed growth after drug washout.

independent). We tested whether glycolysis-generated ATP is sufficient to allow cells to survive during exposure to bedaquiline by performing time-lapse experiments on cells growing in minimal medium supplemented with glucose rather than acetate as the sole source of carbon and energy. In contrast to acetate-grown cells, exposure of glucose-grown cells to bedaquiline had a much smaller impact on intracellular ATP levels, and cells continued to grow and divide in the presence of the compound (Fig. 5; also, see Movie S8 in the supplemental material), suggesting that ATP synthase activity is not essential under these conditions.

DISCUSSION

The emergence and global spread of bacterial antibiotic resistance poses a growing threat to public health. As conventional antibiot-

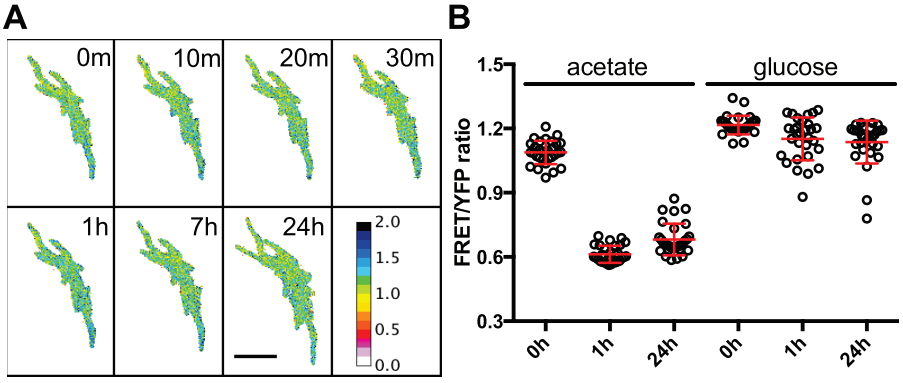

FIG 5 Glucose-grown cells are refractory to bedaquiline-mediated growth inhibition and killing. WT_MA cells were cultured in minimal-acetate or minimal-glucose flow medium in a microfluidic device for ~24 h before addition of bedaquiline (5 μg/ml) at time zero. Phase-contrast and fluorescence images were recorded at 10-min intervals during a 24-h antibiotic exposure period. See Movies S1 and S8 in the supplemental material. (A) Ratiometric FRET/YFP images of cells grown in minimal-glucose flow medium and exposed to bedaquiline starting at time zero. Numbers indicate elapsed time. Scale bar, 5 μm. (B) FRET/YFP ratios of cells grown in minimal-acetate or minimal-glucose flow medium and exposed to bedaquiline starting at time zero. Red lines indicate means ± SD (n = 30 per group).

ics become increasingly ineffective, there is an urgent need for development of new antibiotics with novel targets and mechanisms of action. An exemplar is the ATP synthase inhibitor bedaquiline, which was discovered in cell-based high-throughput screening for compounds active against *M. smegmatis* (4), a nonpathogenic relative of *M. tuberculosis*. In cell-based screens, growth inhibition and PI staining are commonly used to assess the antibacterial activity of novel compounds (4, 34). In a recent study, it was shown that the total ATP content of bacterial cultures can be used as an alternative readout for high-throughput screening (35). Compared to these established methods of evaluating the impact of antibiotics on bacterial vitality, the system described here offers some important advantages.

In contrast to conventional assays, which provide static measurements of ensemble-averaged behavior, biosensor-based ATP measurements can be made repeatedly on the same individual cells and with high temporal resolution throughout the time course of antibiotic exposure and postantibiotic recovery. These unique advantages allowed us to determine that antibiotic-induced ATP switching is a fast, all-or-nothing, and irreversible event that is correlated with immediate growth arrest at the single-cell level. The resulting bimodal distribution of cellular ATP content demonstrates that a 50% reduction of "average" ATP content at the population level actually reflects 100% ATP switching in 50% of cells, rather than 50% reduced ATP levels in 100% of cells. Importantly for potential applications in drug discovery, we found that the timing of ATP switching is remarkably heterogeneous between individuals and that it is a highly reliable real-time predictor of individual cell death. Indeed, as shown here, ATP switching is an earlier and more reliable indicator of antibiotic-mediated killing than conventional PI staining (Fig. 6). Our method can also provide important insights into a compound's mode of action based on the timing of the ATP switch, because rapid switching is consistent with targets that directly affect ATP content, whereas delayed switching corresponds to secondary effects. By comparing cells cultured on specific carbon sources (acetate or glucose), we further defined conditions under which is possible to distinguish compounds that directly affect the activity of ATP synthase.

Fractional killing of bacteria and cancer cells by antibiotics and cytotoxic drugs is a major obstacle to eradicative chemotherapy of infectious and neoplastic diseases, respectively (36, 37). The metabolic status of subpopulations of long-term survivors that are responsible for relapse following antibiotic therapy is a matter of intense debate (38). We find that surviving cells that regrow after

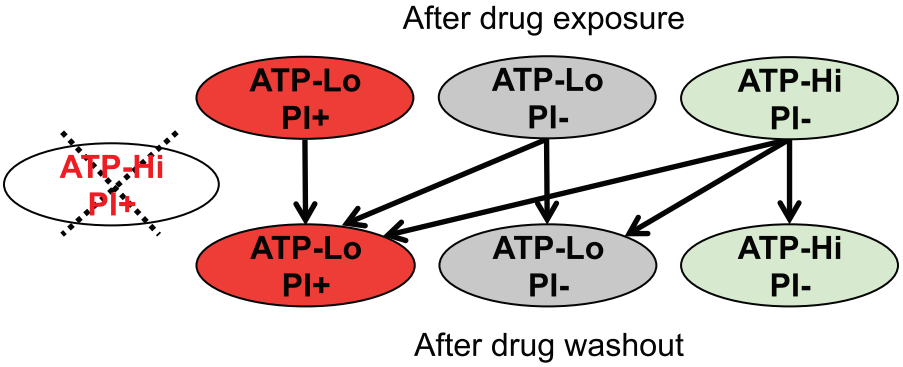

FIG 6 Classification of single-cell fates based on ATP biosensors and PI staining. ATP biosensor tracking and PI staining are compatible and complementary assays for evaluating the physiology and fate of antibiotic-stressed cells. ATP biosensors provide a real-time readout of single-cell energy metabolism. PI staining provides an endpoint readout of single-cell membrane integrity. Simultaneous application of both assays permits the discrimination of three distinct cellular subpopulations: PI-positive/ATP-low cells (red), PI-negative/ATP-low cells (grey), and PI-negative/ATP-high cells (green). (Note that PI-positive cells are always ATP low.) Only ATP-high cells have the potential to resume growth and division after antibiotic washout. Arrows indicate possible transitions after antibiotic washout.

antibiotic washout have invariably maintained high ATP content throughout the period of antibiotic exposure, which is consistent with the idea that these surviving cells are metabolically active (8, 28, 39, 40). Unexpectedly, we identified a substantial fraction of cells that remain intact (PI negative) and metabolically active (ATP high) yet fail to resume growth after antibiotic washout. This cryptic subpopulation of cells could not be identified using conventional assays that rely on bulk measurements or bacterial multiplication, which underscores the important advantages of single-cell techniques such as time-lapse microscopy (8) and flow cytometry (40). Further work is needed to ascertain whether these nongrowing but metabolically active (NGMA) cells are dead or merely dormant. This issue is clinically relevant, as "unculturable" forms of *M. tuberculosis* have been implicated in bacteriological relapse following apparently eradicative chemotherapy (7).

Here we have demonstrated some of the advantages of our method for real-time single-cell measurements of bacterial ATP content as a novel tool for antimicrobial drug discovery. Although we developed this method to investigate antibiotic effects in mycobacteria, we see no major obstacle to applying the same approach to other bacteria and other environmental stressors. When appropriate, more-subtle ATP shifts could be measured using biosensors with altered dynamic ranges, as ATP affinity can be fine-tuned by mutating the ATP-binding domain (23). Moreover, by expressing ATP biosensors in pathogenic bacteria, it might be possible in future to monitor the dynamics of bacterial ATP metabolism during the course of infection.

MATERIALS AND METHODS

Bacterial strains and culture conditions. *M. smegmatis* mc^2155 (wild-type) and derivative strains were grown at 37°C in Middlebrook 7H9 (Difco) liquid medium supplemented with 10% albumin-dextrose-saline (ADS) (BD Biosciences), 0.5% glycerol, and 0.05% Tween 80, Middlebrook 7H10 (Difco) solid medium supplemented with 10% oleic acid-albumin-dextrose-catalase (OADC) (BD Biosciences) and 0.5% glycerol, or Luria-Bertani (LB) solid medium. Frozen stocks were prepared by growing liquid cultures to mid-exponential phase (optical density at 600 nm [OD_{600}] of 0.6 to 0.8), adding glycerol to a 15% final concentration, and storing aliquots at −80°C. For time-lapse experiments bacteria were grown for 3 days at 37°C in M9 minimal medium consisting of M9 salts (Sigma), 2 mM $MgSO_4$, and 0.1 mM $CaCl_2$ supplemented with either 0.5% acetate or 0.5% glucose (minimal-acetate or minimal-glucose). Frozen stocks were prepared by growing minimal-acetate or minimal-glucose cultures to mid-exponential phase and storing aliquots at −80°C. For time-lapse microscopy experiments, aliquots were diluted 10-fold and grown to an OD_{600} of ~0.3 to 0.5.

ATP biosensors. ATP biosensor plasmids pRSET-ATeam3.10 (K_d = 7.4 μM), pRSET-ATeam1.03^{YEMK} (K_d = 1.2 mM), and pRSET-ATeam1.03^{KK} (K_d > 10 mM) were used as templates for PCR amplification to introduce the mycobacterial Shine-Dalgarno sequence and start codon. The forward primer for all three ATeam constructs was 5′ TTAA TTAAGAAGGAGATATACATATGCGGGGTTCTCATCATC 3′. The reverse primer for pRSET-ATeam3.10 was 5′ AGTACTTCACTTGTACAG CTCGTCCATGC 3′. The reverse primer for ATeam1.03^{YEMK} and pRSET-ATeam1.03^{KK} was 5′ AGTACTCAAGCTTACTCGATGTTGTG GC 3′. PCR products were restricted with PacI and ScaI and ligated into the integrating shuttle vector pND235 (which contains the mycobacteriophage L5 *attP-int* sequences) downstream of a strong constitutive mycobacterial promoter. Plasmids were electroporated into *M. smegmatis*, and transformants were selected on LB solid medium supplemented with 50 μg/ml kanamycin.

Construction of an F420-deficient strain of *M. smegmatis* (Δ*fbiC*). An *M. smegmatis* strain with an in-frame deletion of the *fbiC* (MSMEG_5126) gene was constructed using a two-step homologous recombination strategy (41). The recombination template was constructed by PCR amplification of ~800-bp fragments upstream of the *fbiC* start codon (fragment A) and downstream of the *fbiC* stop codon (fragment B). Primers were designed to introduce 5′ PacI and 3′ AvrII sites into fragment A and 5′ AvrII and 3′ AscI sites into fragment B. The reverse primers for amplification of the upstream regions were designed with an AvrII restriction site in-frame with the start codon. The forward primers for amplification of the downstream regions were designed with an AvrII restriction site in-frame with the stop codon. Amplicons were restricted and ligated into unique PacI and AscI sites of the suicide vector pJG1100, which contains *aph* (kanamycin resistance), *hyg* (hygromycin resistance), and *sacB* (sucrose sensitivity) markers (41, 42). The resulting plasmid (pZM217) was verified by DNA sequencing. pZM217 was electroporated into *M. smegmatis*, and transformants were selected on 7H10 solid medium containing 50 μg/ml hygromycin and 25 μg/ml kanamycin. Individual colonies were picked, grown in 7H9 liquid medium (no antibiotic), and then plated on 7H10 solid medium containing 5% sucrose to select for cells in which plasmid excision had occurred. Individual colonies were picked, and the deletion of *fbiC* was confirmed by PCR analysis. The absence of the F420 coenzyme in the Δ*fbiC* strain was confirmed by high-performance liquid chromatography (HPLC) (43).

Time-lapse microscopy. Bacteria were grown to mid-exponential phase in M9 minimal medium consisting of M9 salts (Sigma), 2 mM $MgSO_4$, 0.1 mM $CaCl_2$ supplemented with either 0.5% acetate or 0.5% glucose (minimal-acetate or minimal-glucose) at 37°C, concentrated 10-fold, and cultured in a custom-made microfluidic device at 37°C, as described previously (28). Where noted, the flow medium contained 5 μg/ml bedaquiline, 500 μg/ml isoniazid, 125 μg/ml streptomycin, 200 μg/ml rifampin, or 2.5 μg/ml ciprofloxacin. Images were recorded with a CoolSnap HQ2 charge-coupled device (CCD) camera on phase-contrast, CFPex-YFPem (FRET), and YFPex-YFPem (YFP) channels at 10-min intervals using a DeltaVision personal DV microscope (Applied Precision) equipped with a 100× oil immersion objective and a xenon lamp. Fluorescence images were obtained using a FRET CFP/YFP HC filter set (BrightLine HC 438/24, 542/27; HC beam splitter BS 458) and YFP exciter (AHF Analysentechnik 515/10). Exposure times and neutral density filters were 0.1 s and 50% for phase contrast, 0.3 s and 32% for FRET (CFP/YFP), and 0.1 s and 10% for YFP. Propidium iodide (PI) staining was performed using 0.4 μM red PI (Invitrogen) for 30 min. Images were acquired using an exposure time of 0.1 s with a 50% neutral density filter in combination with an mCherry filter set (excitation filter, 575/25; emission filter, 632/60). All experiments were repeated at least two times with similar results for ~100 microcolonies.

Image processing and single-cell analysis. Images acquired using Resolve3D softWoRx-Acquire version 4.0.0 (Applied Precision) were exported as 16-bit TIFF files and processed using ImageJ 1.46 (NIH) and BactImAS (44). Background was subtracted from each fluorescence channel by deducting the fluorescence in a cell-free area. Image stacks were aligned using a custom-made plugin, Stackreg (http://bigwww.epfl.ch/thevenaz/stackreg/). FRET/YFP ratios were calculated using Ratio Plus (http://rsbweb.nih.gov/ij/plugins/ratio-plus.html). For ratiometric movies, Ratio Plus was modified to use clipping on FRET images based on the YFP background. FRET/YFP ratiometric values of >2 are represented by the upper bound of the range. Single-cell time traces were obtained by tracking background-subtracted intracellular fluorescence on FRET and YFP channels in a large area within the contours of a single cell.

Single-cell measurements of intracellular ATP. Previously, ATeam biosensors have been used for live-cell ATP measurements for no longer than 7 h (26), which is insufficient for assessment of the impact of antibiotics on bacterial cells. A common effect of antibiotic exposure is inhibition of *de novo* protein synthesis, which could lead to a gradual decline in the level of the ATeam protein. Ratiometric (FRET/YFP) measurements should be insensitive to the absolute levels of reporter protein in the cell, since the same protein is responsible for both signals, unless reporter-

derived fluorescence falls below background fluorescence. In cells that had been exposed to bedaquiline for more than 24 h, we found that there was a slow increase in the measured FRET/YFP ratio (Fig. 2A and C), which could be due to a low signal-to-noise (background) ratio when there is not much fluorescent reporter left in the cell (Fig. 2A and C; also, see Fig. S2A in the supplemental material). Total fluorescence of a single cell comprises biosensor fluorescence and two sources of background fluorescence: autofluorescence present within cells and background fluorescence in a cell-free image area. Despite subtracting the out-of-cell fluorescence for every image, small variations within an image remained (<3 arbitrary units [AU] for the FRET channel and <1 AU for the YFP channel). In addition, even in the Δ*fbiC* strain, a minor but measurable level of autofluorescence remained on the FRET channel (Fig. 2D), while autofluorescence on the YFP channel was close to zero (see Fig. S1E). As long as fluorescence intensities were high, the FRET/YFP ratio was not significantly affected by autofluorescence and background fluorescence. As fluorescence intensities decreased over time in the absence of new protein synthesis, the signal from the fluorescent reporter approached background levels and the FRET/YFP ratio became sensitive to details of background subtraction. We therefore measured FRET/YFP ratios only as long as the FRET signal was at least 4-fold higher than observed variation in out-of-cell background fluorescence, and we applied a cutoff in all ratiometric images. We also limited antibiotic exposure in most of our experiments to 24 h in order to ensure the accuracy of our FRET/YFP measurements in single cells.

Fluorescence emission scans. Fluorescence of wild-type and Δ*fbiC* strains of *M. smegmatis* was recorded in 7H9 liquid medium at 24°C with a Tecan Infinite M200 microplate reader as previously described (31). Values were corrected by subtracting the background fluorescence of the 7H9 liquid medium.

Bulk measurements of intracellular ATP. A BacTiter-Glo microbial cell viability assay kit (Promega) was used for bulk measurements of intracellular ATP. WT_MA cells were grown to mid-exponential phase in minimal-acetate medium at 37°C, collected by centrifugation, resuspended in fresh minimal-acetate medium (1:30), and incubated at 37°C for 2 h before addition of 5 μg/ml bedaquiline. Aliquots (70 μl) of bacteria were collected at various time points, mixed with an equal volume of BacTiter-Glo reagent in 96-well white microtiter plates, and incubated 5 min in the dark with shaking before total luminescence was measured with a Tecan F200 microplate reader. Background luminescence was measured by performing the same procedure on aliquots of culture supernatant after removal of cells by filtration through a 0.22-μm-pore filter. Intracellular ATP was calculated by subtracting background luminescence from total luminescence. ATP standards (0.1 nM to 1.0 μM) were assayed in parallel.

Antibiotic sensitivity tests. Sensitivity of wild-type and Δ*fbiC* strains of *M. smegmatis* to bedaquiline (Janssen Infectious Diseases & Vaccines), isoniazid (Sigma), streptomycin (Sigma), rifampin (Sigma), and ciprofloxacin (Sigma) was determined using a broth microdilution assay (45). Aliquots (2 ml) of 7H9 liquid medium containing 2-fold serial dilutions of bedaquiline, isoniazid, rifampin, streptomycin, or ciprofloxacin were inoculated with 2 ml of mid-exponential-phase cultures of *M. smegmatis* to a final OD_{600} of ~0.002. OD_{600} values were determined after 24 h of incubation at 37°C with aeration. Sigmoidal dose-response (variable slope) nonlinear fit was calculated using GraphPad Prism 5.0 (GraphPad Software).

Statistical analysis. Probabilities that a PI-positive cell will be ATP high and that a growing cell will be ATP low were calculated with the 95% confidence interval of the rate, given that nothing showed up in N trials, where the upper limit is found by taking binomial probability of zero hits in *n* trials. Pearson's test was used to evaluate the sibling pair correlations of ATP switching (see Fig. S2B in the supplemental material). Unpaired *t* tests with equal standard deviations were used for comparisons between different time points (see Fig. S2D). *P* values were calculated using GraphPad Prism 5.0 (GraphPad Software), and values of <0.05 were considered significant.

SUPPLEMENTAL MATERIAL

Supplemental material for this article may be found at http://mbio.asm.org/lookup/suppl/doi:10.1128/mBio.02236-14/-/DCSupplemental.

Figure S1, EPS file, 1.2 MB.
Figure S2, EPS file, 1.6 MB.
Movie S1, MOV file, 13.9 MB.
Movie S2, MOV file, 14.5 MB.
Movie S3, MOV file, 18.2 MB.
Movie S4, MOV file, 21.2 MB.
Movie S5, MOV file, 17.6 MB.
Movie S6, MOV file, 18.7 MB.
Movie S7, MOV file, 21.2 MB.
Movie S8, MOV file, 8.4 MB.

ACKNOWLEDGMENTS

We thank H. Imamura (ISIR, Osaka University) for providing the ATeam plasmids, N. Dhar for providing shuttle vector pND235, K. Andries (Janssen Infectious Diseases & Vaccines) for providing bedaquiline, D. Mekterović, A. Seitz, and A. Radenović for helpful discussions, and A. Tischler for critical reading of the manuscript.

This research was funded in part by grants to J.D.M. from the Swiss National Science Foundation (no. 310030_156945) and the Innovative Medicines Initiative (no. 115337), a joint undertaking of the European Union Seventh Framework Programme and EFPIA (http://www.imi.europa.eu/).

Ž.M. and J.D.M. conceived the study and designed the experiments. Ž.M. performed the experiments and analyzed the data. E.Ö. subcloned ATeam plasmids and provided ideas. Ž.M. and J.D.M. wrote the manuscript.

REFERENCES

1. **Lewis K.** 2013. Platforms for antibiotic discovery. Nat Rev Drug Discov **12**:371–387. http://dx.doi.org/10.1038/nrd3975.
2. **Payne DJ, Gwynn MN, Holmes DJ, Pompliano DL.** 2007. Drugs for bad bugs: confronting the challenges of antibacterial discovery. Nat Rev Drug Discov **6**:29–40. http://dx.doi.org/10.1038/nrd2201.
3. **Anonymous.** 2010. The antibacterial lead discovery challenge. Nat Rev Drug Discov **9**:751–752. http://dx.doi.org/10.1038/nrd3289.
4. **Andries K, Verhasselt P, Guillemont J, Göhlmann HW, Neefs JM, Winkler H, Van Gestel J, Timmerman P, Zhu M, Lee E, Williams P, de Chaffoy D, Huitric E, Hoffner S, Cambau E, Truffot-Pernot C, Lounis N, Jarlier V.** 2005. A diarylquinoline drug active on the ATP synthase of Mycobacterium tuberculosis. Science **307**:223–227. http://dx.doi.org/10.1126/science.1106753.
5. **Zumla AI, Gillespie SH, Hoelscher M, Philips PP, Cole ST, Abubakar I, McHugh TD, Schito M, Maeurer M, Nunn AJ.** 2014. New antituberculosis drugs, regimens, and adjunct therapies: needs, advances, and future prospects. Lancet Infect Dis **14**:327–340. http://dx.doi.org/10.1016/S1473-3099(13)70328-1.
6. **Maisonneuve E, Gerdes K.** 2014. Molecular mechanisms underlying bacterial persisters. Cell **157**:539–548. http://dx.doi.org/10.1016/j.cell.2014.02.050.
7. **Manina G, McKinney JD.** 2013. A single-cell perspective on non-growing but metabolically active (NGMA) bacteria. Curr Top Microbiol Immunol **374**:135–161. http://dx.doi.org/10.1007/82_2013_333.
8. **Manina G, Dhar N, McKinney JD.** Stress and host immunity amplify M. tuberculosis heterogeneity and induce non-growing metabolically active forms. Cell Host Microbe **17**:32–46. http://dx.doi.org/10.1016/j.chom.2014.11.016.
9. **Newman RH, Fosbrink MD, Zhang J.** 2011. Genetically encodable fluorescent biosensors for tracking signaling dynamics in living cells. Chem Rev **111**:3614–3666. http://dx.doi.org/10.1021/cr100002u.
10. **Okumoto S, Jones A, Frommer WB.** 2012. Quantitative imaging with fluorescent biosensors. Annu Rev Plant Biol **63**:663–706. http://dx.doi.org/10.1146/annurev-arplant-042110-103745.
11. **Ewald JC, Reich S, Baumann S, Frommer WB, Zamboni N.** 2011.

Engineering genetically encoded nanosensors for real-time in vivo measurements of citrate concentrations. PLoS One **6:**e28245. http://dx.doi.org/10.1371/journal.pone.0028245.

12. **Potzkei J, Kunze M, Drepper T, Gensch T, Jaeger KE, Büchs J.** 2012. Real-time determination of intracellular oxygen in bacteria using a genetically encoded FRET-based biosensor. BMC Biol **10:**28. http://dx.doi.org/10.1186/1741-7007-10-28.
13. **Kaper T, Lager I, Looger LL, Chermak D, Frommer WB.** 2008. Fluorescence resonance energy transfer sensors for quantitative monitoring of pentose and disaccharide accumulation in bacteria. Biotechnol Biofuels **1:**11. http://dx.doi.org/10.1186/1754-6834-1-11.
14. **Yaginuma H, Kawai S, Tabata KV, Tomiyama K, Kakizuka A, Komatsuzaki T, Noji H, Imamura H.** 2014. Diversity in ATP concentrations in a single bacterial cell population revealed by quantitative single-cell imaging. Sci Rep **4:**6522. http://dx.doi.org/10.1038/srep06522.
15. **Christen M, Kulasekara HD, Christen B, Kulasekara BR, Hoffman LR, Miller SI.** 2010. Asymmetrical distribution of the second messenger c-di-GMP upon bacterial cell division. Science **328:**1295–1297. http://dx.doi.org/10.1126/science.1188658.
16. **Pethe K, Bifani P, Jang J, Kang S, Park S, Ahn S, Jiricek J, Jung J, Jeon HK, Cechetto J, Christophe T, Lee H, Kempf M, Jackson M, Lenaerts AJ, Pham H, Jones V, Seo MJ, Kim YM, Seo M, Seo JJ, Park D, Ko Y, Choi I, Kim R, Kim SY, Lim S, Yim SA, Nam J, Kang H, Kwon H, Oh CT, Cho Y, Jang Y, Kim J, Chua A, Tan BH, Nanjundappa MB, Rao SP, Barnes WS, Wintjens R, Walker JR, Alonso S, Lee S, Oh S, Oh T, Nehrbass U, Han SJ, No Z, Lee J, Brodin P, Cho SN, Nam K.** 2013. Discovery of Q203, a potent clinical candidate for the treatment of tuberculosis. Nat Med **19:**1157–1160. http://dx.doi.org/10.1038/nm.3262.
17. **Petersen C, Møller LB.** 2000. Invariance of the nucleoside triphosphate pools of Escherichia coli with growth rate. J Biol Chem **275:**3931–3935. http://dx.doi.org/10.1074/jbc.275.6.3931.
18. **Parrish NM, Ko CG, Hughes MA, Townsend CA, Dick JD.** 2004. Effect of n-octanesulphonylacetamide (OSA) on ATP and protein expression in Mycobacterium bovis BCG. J Antimicrob Chemother **54:**722–729. http://dx.doi.org/10.1093/jac/dkh408.
19. **Koul A, Vranckx L, Dendouga N, Balemans W, Van den Wyngaert I, Vergauwen K, Göhlmann HW, Willebrords R, Poncelet A, Guillemont J, Bald D, Andries K.** 2008. Diarylquinolines are bactericidal for dormant mycobacteria as a result of disturbed ATP homeostasis. J Biol Chem **283:**25273–25280. http://dx.doi.org/10.1074/jbc.M803899200.
20. **Rao SP, Alonso S, Rand L, Dick T, Pethe K.** 2008. The protonmotive force is required for maintaining ATP homeostasis and viability of hypoxic, nonreplicating Mycobacterium tuberculosis. Proc Natl Acad Sci U S A **105:**11945–11950. http://dx.doi.org/10.1073/pnas.0711697105.
21. **Gengenbacher M, Rao SP, Pethe K, Dick T.** 2010. Nutrient-starved, non-replicating Mycobacterium tuberculosis requires respiration, ATP synthase and isocitrate lyase for maintenance of ATP homeostasis and viability. Microbiology **156:**81–87. http://dx.doi.org/10.1099/mic.0.033084-0.
22. **Schneider DA, Gourse RL.** 2004. Relationship between growth rate and ATP concentration in Escherichia coli: a bioassay for available cellular ATP. J Biol Chem **279:**8262–8268. http://dx.doi.org/10.1074/jbc.M311996200.
23. **Imamura H, Nhat KP, Togawa H, Saito K, Iino R, Kato-Yamada Y, Nagai T, Noji H.** 2009. Visualization of ATP levels inside single living cells with fluorescence resonance energy transfer-based genetically encoded indicators. Proc Natl Acad Sci U S A **106:**15651–15656. http://dx.doi.org/10.1073/pnas.0904764106.
24. **Ando T, Imamura H, Suzuki R, Aizaki H, Watanabe T, Wakita T, Suzuki T.** 2012. Visualization and measurement of ATP levels in living cells replicating hepatitis C virus genome RNA. PLoS Pathog **8:**e1002561. http://dx.doi.org/10.1371/journal.ppat.1002561.
25. **Kishikawa J, Fujikawa M, Imamura H, Yasuda K, Noji H, Ishii N, Mitani S, Yokoyama K.** 2012. MRT letter: expression of ATP sensor protein in Caenorhabditis elegans. Microsc Res Tech **75:**15–19. http://dx.doi.org/10.1002/jemt.21103.
26. **Hatsugai N, Perez Koldenkova V, Imamura H, Noji H, Nagai T.** 2012. Changes in cytosolic ATP levels and intracellular morphology during bacteria-induced hypersensitive cell death as revealed by real-time fluorescence microscopy imaging. Plant Cell Physiol **53:**1768–1775. http://dx.doi.org/10.1093/pcp/pcs119.
27. **Lu P, Haagsma AC, Pham H, Maaskant JJ, Mol S, Lill H, Bald D.** 2011. Pyrazinoic acid decreases the proton motive force, respiratory ATP synthesis activity, and cellular ATP levels. Antimicrob Agents Chemother **55:**5354–5357. http://dx.doi.org/10.1128/AAC.00507-11.
28. **Wakamoto Y, Dhar N, Chait R, Schneider K, Signorino-Gelo F, Leibler S, McKinney JD.** 2013. Dynamic persistence of antibiotic-stressed mycobacteria. Science **339:**91–95. http://dx.doi.org/10.1126/science.1229858.
29. **Koul A, Vranckx L, Dhar N, Gohlmann HW, Ozdemir E, Neefs JM, Schulz M, Lu P, Mortz E, McKinney JD, Andries K, Bald D.** 2014. Delayed bactericidal response of Mycobacterium tuberculosis to bedaquiline involves remodelling of bacterial metabolism. Nat Commun **5:**3369.
30. **Hukasova E, Silva Cascales H, Kumar SR, Lindqvist A.** 2012. Monitoring kinase and phosphatase activities through the cell cycle by ratiometric FRET. J Vis Exp **2012:**e3410. http://dx.doi.org/10.3791/3410.
31. **Patiño S, Alamo L, Cimino M, Casart Y, Bartoli F, García MJ, Salazar L.** 2008. Autofluorescence of mycobacteria as a tool for detection of Mycobacterium tuberculosis. J Clin Microbiol **46:**3296–3302. http://dx.doi.org/10.1128/JCM.02183-08.
32. **Choi KP, Kendrick N, Daniels L.** 2002. Demonstration that fbiC is required by Mycobacterium bovis BCG for coenzyme F(420) and FO biosynthesis. J Bacteriol **184:**2420–2428. http://dx.doi.org/10.1128/JB.184.9.2420-2428.2002.
33. **Williams SC, Hong Y, Danavall DCA, Howard-Jones HM, Gibson D, Frischer ME, Verity PG.** 1999. Erratum to "Distinguishing between living and nonliving bacteria: evaluation of the vital stain propidium iodide and its combined use with molecular probes in aquatic samples" [J. Microbiol. Methods 32 (1998) 225–236]. J Microbiol Methods **35:**183–184.
34. **Makarov V, Manina G, Mikusova K, Möllmann U, Ryabova O, Saint-Joanis B, Dhar N, Pasca MR, Buroni S, Lucarelli AP, Milano A, De Rossi E, Belanova M, Bobovska A, Dianiskova P, Kordulakova J, Sala C, Fullam E, Schneider P, McKinney JD, Brodin P, Christophe T, Waddell S, Butcher P, Albrethsen J, Rosenkrands I, Brosch R, Nandi V, Bharath S, Gaonkar S, Shandil RK, Balasubramanian V, Balganesh T, Tyagi S, Grosset J, Riccardi G, Cole ST.** 2009. Benzothiazinones kill Mycobacterium tuberculosis by blocking arabinan synthesis. Science **324:**801–804. http://dx.doi.org/10.1126/science.1171583.
35. **Mak PA, Rao SP, Ping Tan M, Lin X, Chyba J, Tay J, Ng SH, Tan BH, Cherian J, Duraiswamy J, Bifani P, Lim V, Lee BH, Ling Ma N, Beer D, Thayalan P, Kuhen K, Chatterjee A, Supek F, Glynne R, Zheng J, Boshoff HI, Barry CE III, Dick T, Pethe K, Camacho LR.** 2012. A high-throughput screen to identify inhibitors of ATP homeostasis in non-replicating Mycobacterium tuberculosis. ACS Chem Biol **7:**1190–1197. http://dx.doi.org/10.1021/cb2004884.
36. **Helaine S, Kugelberg E.** 2014. Bacterial persisters: formation, eradication, and experimental systems. Trends Microbiol **22:**417–424. http://dx.doi.org/10.1016/j.tim.2014.03.008.
37. **Glickman MS, Sawyers CL.** 2012. Converting cancer therapies into cures: lessons from infectious diseases. Cell **148:**1089–1098. http://dx.doi.org/10.1016/j.cell.2012.02.015.
38. **Balaban NQ, Gerdes K, Lewis K, McKinney JD.** 2013. A problem of persistence: still more questions than answers? Nat Rev Microbiol **11:**587–591. http://dx.doi.org/10.1038/nrmicro3076.
39. **Orman MA, Brynildsen MP.** 2013. Dormancy is not necessary or sufficient for bacterial persistence. Antimicrob Agents Chemother **57:**3230–3239. http://dx.doi.org/10.1128/AAC.00243-13.
40. **Amato SM, Fazen CH, Henry TC, Mok WW, Orman MA, Sandvik EL, Volzing KG, Brynildsen MP.** 2014. The role of metabolism in bacterial persistence. Front Microbiol **5:**70. http://dx.doi.org/10.3389/fmicb.2014.00070.
41. **Pavelka MS, Jr., Jacobs WR, Jr.** 1999. Comparison of the construction of unmarked deletion mutations in Mycobacterium smegmatis, Mycobacterium bovis bacillus Calmette-Guerin, and Mycobacterium tuberculosis H37Rv by allelic exchange. J Bacteriol **181:**4780–4789.
42. **Parish T, Stoker NG.** 2000. Use of a flexible cassette method to generate a double unmarked Mycobacterium tuberculosis tlyA plcABC mutant by gene replacement. Microbiology **146:**1969–1975.
43. **Bair TB, Isabelle DW, Daniels L.** 2001. Structures of coenzyme F(420) in Mycobacterium species. Arch Microbiol **176:**37–43. http://dx.doi.org/10.1007/s002030100290.
44. **Mekterović I, Mekterović D, Maglica Z.** 2014. BactImAS: a platform for processing and analysis of bacterial time-lapse microscopy movies. BMC Bioinformatics **15:**251. http://dx.doi.org/10.1186/1471-2105-15-251.
45. **Andrews JM.** 2001. Determination of minimum inhibitory concentrations. J Antimicrob Chemother **48**(Suppl 1):5–16. http://dx.doi.org/10.1093/jac/48.suppl_1.5.